Imaging Pharmacodynamics of the α-Folate Receptor–Targeted Thymidylate Synthase Inhibitor BGC 945

Radhakrishna G. Pillai,[1] Martin Forster,[2] Meg Perumal,[1] Fraser Mitchell,[2] Julius Leyton,[1] Franklin I. Aibgirhio,[3] Oksana Golovko,[3] Ann L. Jackman,[2] and Eric O. Aboagye[1]

[1]Department of Molecular Therapy, Imperial College London, Faculty of Medicine, Hammersmith Hospital Campus, London, United Kingdom; [2]Section of Medicine, The Institute of Cancer Research, Sutton, Surrey, United Kingdom; and [3]Wolfson Brain Imaging Center, University of Cambridge, Addenbrookes Hospital, Cambridge, United Kingdom

Abstract

The assessment of tissue-specific pharmacodynamics is desirable in the development of tumor-targeted therapies. Plasma deoxyuridine (dUrd) levels, a measure of systemic thymidylate synthase (TS) inhibition, has limited application for studying the pharmacodynamics of novel TS inhibitors targeted to the high affinity α-folate receptor (FR). Here, we have evaluated the utility of [^{18}F]fluorothymidine positron emission tomography ([^{18}F]FLT-PET) for imaging the tissue pharmacodynamics of BGC 945, an FR-targeted antifolate TS inhibitor; the nontargeted antifolate BGC 9331 was used for comparison. TS inhibition by both drugs induced a concentration-dependent increase in [^{3}H]thymidine uptake in FR-positive human epidermoid KB cells. Membrane-associated equilibrative nucleoside transporter type 1 levels increased from 55,720 ± 6,101 to 118,700 ± 5,193 and 130,800 ± 10,800 per cell at 100 μg/mL of BGC 9331 and BGC 945, respectively, suggesting this as a potential mechanism of increased nucleoside uptake. In keeping with these *in vitro* findings, tumor [^{18}F]FLT accumulation in KB xenografts increased by ≥2-fold after drug treatment with maximal levels at 1 to 4 hours and 4 to 24 hours after BGC 9331 and BGC 945 treatment, respectively. Of interest to FR targeting, BGC 9331, but not BGC 945, induced accumulation of [^{18}F]FLT uptake in intestine, a proliferative and TS-responsive tissue. For both drugs, quantitative changes in tumor [^{18}F]FLT uptake were associated with increased tumor dUrd levels. In conclusion, we have validated the utility of [^{18}F]FLT-PET to image TS inhibition induced by antifolates and shown the tumor-specific activity of BGC 945. This imaging biomarker readout will be useful in the early clinical development of BGC 945. [Cancer Res 2008;68(10):3827–34]

Introduction

New agents with unique tumor-targeting properties are being developed in a number of institutions. One such agent, the antifolate BGC 945, selectively binds to the α-folate receptor (α-FR), a cell-surface glycoprotein, with very high affinity similar to that of folic acid (K_D, ~0.1 nmol/L), a natural ligand. It is then transported into cells by receptor-mediated endocytosis, where it acts as a potent inhibitor of thymidylate synthase (TS; K_i TS, 1.4 nmol/L), leading to cell death (1, 2). The α-FR is overexpressed in several cancers, particularly epithelial tumors, such as ovarian carcinoma (up to 90% of cases). However, it has restricted expression in TS-responsive normal proliferating tissues, such as gut and bone marrow, and this expression is limited to the apical surface membrane and therefore not assessable to FR-binding agents in the circulation (3, 4). Compared with other antifolates, such as raltitrexed and plevitrexed (BGC 9331), which are taken up into cells predominantly via the ubiquitous reduced folate carrier (RFC; ref. 5), BGC 945 has the potential to have a particularly high therapeutic index because of reduced activity on normal TS-responsive tissues. However, this efficacy is likely to be seen only in patients with tumors expressing the α-FR.

Pharmacodynamic biomarkers that report on modulation of a biological target and help define a biologically effective dose are increasingly being incorporated into early clinical development of targeted anticancer agents. With respect to TS inhibition, the most widely accepted biomarker is increased plasma deoxyuridine (dUrd) levels measured by high-performance liquid chromatography (HPLC) or liquid chromatography–mass spectrometry (6, 7). Elevated plasma dUrd, however, mainly reflects systemic TS inhibition in normal proliferating tissues rather than on tumor alone. This assay has been adapted to measure tumor dUrd levels and will be appropriate for BGC 945, but this will involve multiple core biopsies in clinical trials and hence be inconvenient for patient studies. Recently, our group reported a novel method for imaging TS inhibition by noninvasive positron emission tomography (PET; ref. 8). A unique biochemistry of tissues in which TS inhibition leads to redistribution of the nucleoside transporter ENT1 to the cell membrane, provided the basis for using [^{18}F]fluorothymidine ([^{18}F]FLT)–PET to image 5-fluorouracil–induced TS inhibition (8). In this manuscript, we have validated this imaging method for antifolates with BGC 9331 in time and dose and used the method for the first time to quantitatively evaluate tissue-specific TS inhibition by the antifolate BGC 945.

Materials and Methods

Antifolates and radiopharmaceutical. BGC 945 (as the 6-*S*-trifluoroacetic acid salt; ref. 2) and BGC 9331 were supplied by BTG International. BGC 9331 was a 10 mmol/L solution, stored at 4°C, and used within recommended storage dates for each batch. BGC 945 was provided in solid form, dissolved in 0.15 mol/L $NaHCO_3$ for *in vitro* use, and stored at −20°C as a 10 mmol/L solution for up to 3 mo. For *in vivo* use, BGC 945 was dissolved in 0.05 mol/L $NaHCO_3$, and the pH of the dose solution was adjusted to ~9 by addition of 1 mol/L NaOH. [^{18}F]FLT was synthesized by radiofluorination of the 3-*N*-Boc-5′-*O*-dimethoxytrityl-3′-*O*-nosyl-thymidine precursor using a GE TracerLab MX synthesis module (GE Healthcare UK

Note: Supplementary data for this article are available at Cancer Research Online (http://cancerres.aacrjournals.org/).

R.G. Pillai and M. Forster contributed equally to this work.

Requests for reprints: Eric O. Aboagye, Molecular Therapy and PET Oncology Research Group, Imperial College London, Faculty of Medicine, Hammersmith Hospital, Room 240, MRC Cyclotron Building, Du Cane Road, London, W12 ONN, United Kingdom. Phone: 44208-383-3759; Fax: 44208-383-1783; E-mail: eric.aboagye@imperial.ac.uk.

doi:10.1158/0008-5472.CAN-08-0135

Limited) based on a method previously described by Oh et al. (9). All samples had >98% radiochemical purity as determined by HPLC with radiochemical detection (radio-HPLC), and the specific radioactivity was 120 to 150 GBq/μmol at the end of synthesis. [Methyl-^{3}H]Thymidine ([^{3}H]Thd; 925 GBq/mmol, 37 MBq/mL) and [5-^{3}H]-dUrd (925 GBq/mmol, 37 MBq/mL) were purchased from GE Healthcare UK Limited. [^{3}H]Nitrobenzyl mercaptopurine ribonucleoside ([^{3}H]NBMPR; also known as [^{3}H]*S*-(*p*-nitrobenzyl)-6-thioinosine; 555 GBq/mmol, 37 MBq/mL) was purchased from Moravek Biochemicals, Inc.

Intrinsic uptake of nucleosides by tumor cells. [^{3}H]Thd was used to assess TS-induced nucleoside uptake in cultured cells. For this, α-FR–positive human epidermoid KB cells (10) were grown in folate-free RPMI 1640 (Life Technologies) supplemented with 10% heat-inactivated dialysed FCS (PAA Laboratories) and antibiotics in T75 tissue culture flasks at a seeding density of 0.5×10^6 (5% CO_2 incubator; 37°C). Leucovorin (*RS*-5-formyl tetrahydrofolic acid) was added to the growth medium to a final concentration of 20 nmol/L to approximate the concentration of folates in human plasma. At ~60% confluence, the cells were exposed to increasing concentrations (0.1–500 μg/mL) of BGC 9331 and BGC 945 in growth media for 2 h. Drug-containing medium was removed, and the cells were then washed and pulsed with [^{3}H]Thd (0.37 MBq/flask) for 1 h to determine whole cell and DNA associated radioactivity as previously reported (8). Data were quench-corrected and expressed as counts per minute per microgram protein for whole cell and counts per minute per microgram DNA for DNA.

Kinetics of nucleoside transport. Exponentially growing KB cells were treated for 2 h with BGC 9331 or BGC 945 at concentrations of 10 or 100 μg/mL or equal volume of vehicle (PBS). Single cells prepared by trypsinization were kept suspended in culture medium by mild agitation with a shaker. Plasma membrane NBMPR-sensitive nucleoside transporter binding sites (a measure of membrane ENT1; ref. 8) on KB cells were measured by incubation of 2×10^6 cells with 0.1, 0.25, 0.5,1, 2, 4, 8, 16, 32, and 48 nmol/L of [^{3}H]NBMPR in the medium. The total incubation volume was 400 μL, and the studies were carried out at room temperature (~20°C) for 60 min (equilibrium binding). In parallel experiments, to assess nonspecific binding, equal numbers of cells were preincubated with 20 μmol/L of the specific inhibitor nitrobenzylthioguanosine for 15 min and then incubated with [^{3}H]NBMPR at the same concentration range as above. To analyze whether the increase in nucleoside transport was due to increases in cellular synthesis of the transporter protein, similar experiments were conducted on cells pretreated for 15 min with cycloheximide (10 μg/mL). At the end of incubation, all reactions were quickly stopped and processed, as previously reported (8). Specific binding (binding sites per cell) was defined as the difference in [^{3}H]NBMPR content in the presence and absence of nitrobenzylthioguanosine. The maximal binding (B_{max}; the number of transporters) and the concentration of ligand required to reach half-maximal binding (K_D; affinity) were determined by curve fitting using GraphPad Prism, version 4 (GraphPad). Data were fitted to the equation, $Y = B_{am} \times X / (K_D + X)$, wherein Y and X are the specific binding and [^{3}H]NBMPR concentration (in nmol/L), respectively. Experiments were performed in triplicate.

Animals, tumor model, and drug treatment. The tumor model used in this study was the α-FR–positive KB xenograft grown in BALB/c nu/nu mice. For this procedure, KB tumor cells cultured as described above were harvested and resuspended in unsupplemented RPMI 1640 at 5×10^7 cells/mL. Tumors were induced by s.c. injection of 5×10^6 cells in 50 μL of the cell suspension into the back of 6-wk-old to 8-wk-old female BALB/c nu/nu mice obtained from Harlan United Kingdom Ltd. Tumor dimensions were measured continuously using a caliper, and tumor volumes were calculated by the equation, volume = $(\pi / 6) \times a \times b \times c$, wherein *a, b*, and *c* represent three orthogonal axes of the tumor. The tumors attained a size of ~100 mm^3 at ~14 d later. Given that normal mouse chow is supplemented with high concentrations of folic acid and consequently mice have high plasma folate levels (~5-fold to 10-fold higher than humans) that may reduce BGC 945 binding to FR, mice that were to be treated with BGC 945 were fed mouse chow unsupplemented with folic acid (supplied as pellets from TestDiet) starting 5 d before the inoculation of KB cells and then throughout the tumor growth and drug treatment phase until imaging studies were done in an attempt to reduce folate levels to that found in humans (11, 12). Because BGC 9331 is predominantly transported by the high-capacity RFC, studies with this compound were performed under normal dietary conditions, as has been reported by other investigators (5, 13, 14); to allow for direct comparison, imaging studies were also performed after vehicle or BGC 9331 injection (100 mg/kg; 4 h posttreatment) in a separate cohort of mice fed chow unsupplemented with folic acid. Mice were treated with drug and/or used for imaging studies when their tumors reached ~100 mm^3. For imaging studies, size-matched tumor-bearing mice were randomized and given a single 100 mg/kg injection of BGC 9331 or BGC 945 i.p. and imaged at different times after drug injection (vehicle, 1, 4, 24, and 48 h) to assess the time course of target modulation. Images were also acquired 4 h after a range of different doses of each compound was given (vehicle, 25, 50, 100, 150, and 200 mg/kg). All animal work was performed by licensed investigators in accordance with the Guidance on the Operation of Animals (Scientific Procedures) Act 1986 of United Kingdom (HMSO, London, UK, 1990) and in full compliance with government regulations and guidelines on the welfare of animals in experimental neoplasia (15).

PET studies. [^{18}F]FLT-PET studies were carried out on a dedicated small animal PET scanner, quad-HIDAC (Oxford Positron Systems; refs. 8, 16, 17). For scanning, the tail veins of vehicle-treated, BGC 9331–treated, or BGC 945–treated mice were cannulated after induction of anesthesia with isofluorane-O_2-N_2O mixture. The animals were placed within a thermostatically controlled jig and positioned prone in the scanner. The jig was calibrated to provide a rectal temperature of ~37°C. A bolus injection of [^{18}F]FLT (2.96–3.7 MBq) was given i.v. via the tail vein cannula, and scanning commenced. Dynamic scans were acquired in list-mode format over a 60-min period without attenuation correction. The acquired data were sorted into 0.5-mm sinogram bins and 19 time frames ($0.5 \times 0.5 \times 0.5$ mm voxels; 4×15, 4×60, and 11×300 s) for image reconstruction, which was performed by filtered back-projection using a two-dimensional Hamming filter (cutoff 0.6). The image data sets obtained were visualized using the Analyze software (version 6.0; Biomedical Imaging Resource, Mayo Clinic).

Image analysis and quantification of radiotracer uptake. Cumulative images comprising of 30 to 60 min of the dynamic data were used for visualization of radiotracer uptake and to draw regions of interest. Regions of interest (each 0.5-mm thickness) were defined on five slices of tumor, small intestine (as an example of a proliferative TS-responsive normal tissue), and heart (blood volume; ref. 17). Dynamic data from these slices were averaged for each tissue and at each of the 19 time points to obtain time versus radioactivity curves for these tissues. Tissue radioactivity was normalized to that of heart to obtain a normalized uptake value (NUV). The NUV at 60 min postinjection (NUV_{60}) was used for comparisons. The area under the NUV curve (AUC) was calculated as the integral of NUV from 0 to 60 min. The fractional retention of tracer (FRT) at 60 min relative to that at 2.5 min was also calculated.

Analysis of tumor thymidine kinase 1 protein and cofactor levels. Thymidine kinase 1 (TK1) protein and cofactor (ATP) levels were assessed by Western blot and bioluminescence assays, respectively. KB tumors were excised from a cohort of mice treated with PBS or 100 mg/kg of the drug at 2 h postinjection and snap-frozen in liquid nitrogen. Tumors were pulverized in liquid nitrogen and homogenized in ice-cold Dulbecco's PBS using an Ultra-Thurrax homogenizer (IKA). TK1 levels were then analyzed by Western blot as previously described (8). ATP levels were determined by a bioluminescence assay as previously described (8) using the same supernatants used for the Western blots above.

Analysis of tumor dUrd levels. KB tumors were taken from mice immediately after the imaging studies, snap-frozen in liquid nitrogen, and stored at −80°C until use. To confirm that TS was inhibited by BGC 9331 and BGC 945, dUrd levels were assessed by a chromatographic assay (7, 8). Briefly, whole (weighed) tumor samples were homogenized and the homogenate initially clarified by perchlorate protein precipitation; after neutralization and centrifugation, the supernatant was further clarified by solid phase extraction. After evaporation to dryness using a vacuum centrifuge, the samples were reconstituted for analysis by HPLC as

Table 1. Effect of BGC 9331 and BGC 945 on ENT1 redistribution to the membrane of KB cells *in vitro*

		Control (n = 3)	10 μg/mL (n = 3)	100 μg/mL (n = 3)
BGC 9331	B_{max} (no. binding sites per cell)*	55,720 ± 6,101	90,430 ± 6,384 †	118,700 ± 5,193 †
	K_D (nmol/L) ‡	5.8 ± 0.4	6.3 ± 0.9	7.7 ± 0.3*
BGC 945	B_{max} (no. binding sites per cell)*	55,720 ± 6,101	95,840 ± 1,340 †	130,800 ± 10,800 †
	K_D (nmol/L)	5.8 ± 0.4	7.1 ± 0.3	7.4 ± 3.0

NOTE: Data are mean ± SD.
One-way ANOVA (all groups; as superscript on variables) and multiple comparison test against control values (Dunnett; as superscript on individual values).
*$P \leq 0.001$.
†$P \leq 0.01$.
‡$P \leq 0.05$.

previously described (7). dUrd was separated on a C18 stationary-phase with a mobile-phase comprising of 0.1% trifluoroacetic acid and detected at 267 nm using a UV-photodiode array detector. dUrd losses from sample preparation were estimated by measuring the recovered activity of [5-^{3}H]-dUrd spiked into blank tumor samples. Chromatographic peak areas for the samples were compared with a calibration curve; data were expressed as nanomoles per gram.

Statistical analysis. Statistical analyses were performed using the software GraphPad Prism, version 4 (GraphPad). Multiple data sets comprising of different time points and dose levels were compared using a one-way analysis of variance; Dunnett's multiple comparison test was used to analyze the significance of the different groups. Two-tailed P values of ≤ 0.05 were considered significant.

Results

BGC 9331 and BGC 945 induce cellular uptake of [^{3}H]Thd. The two TS inhibitors, BGC 9331 and BGC 945, increased the whole

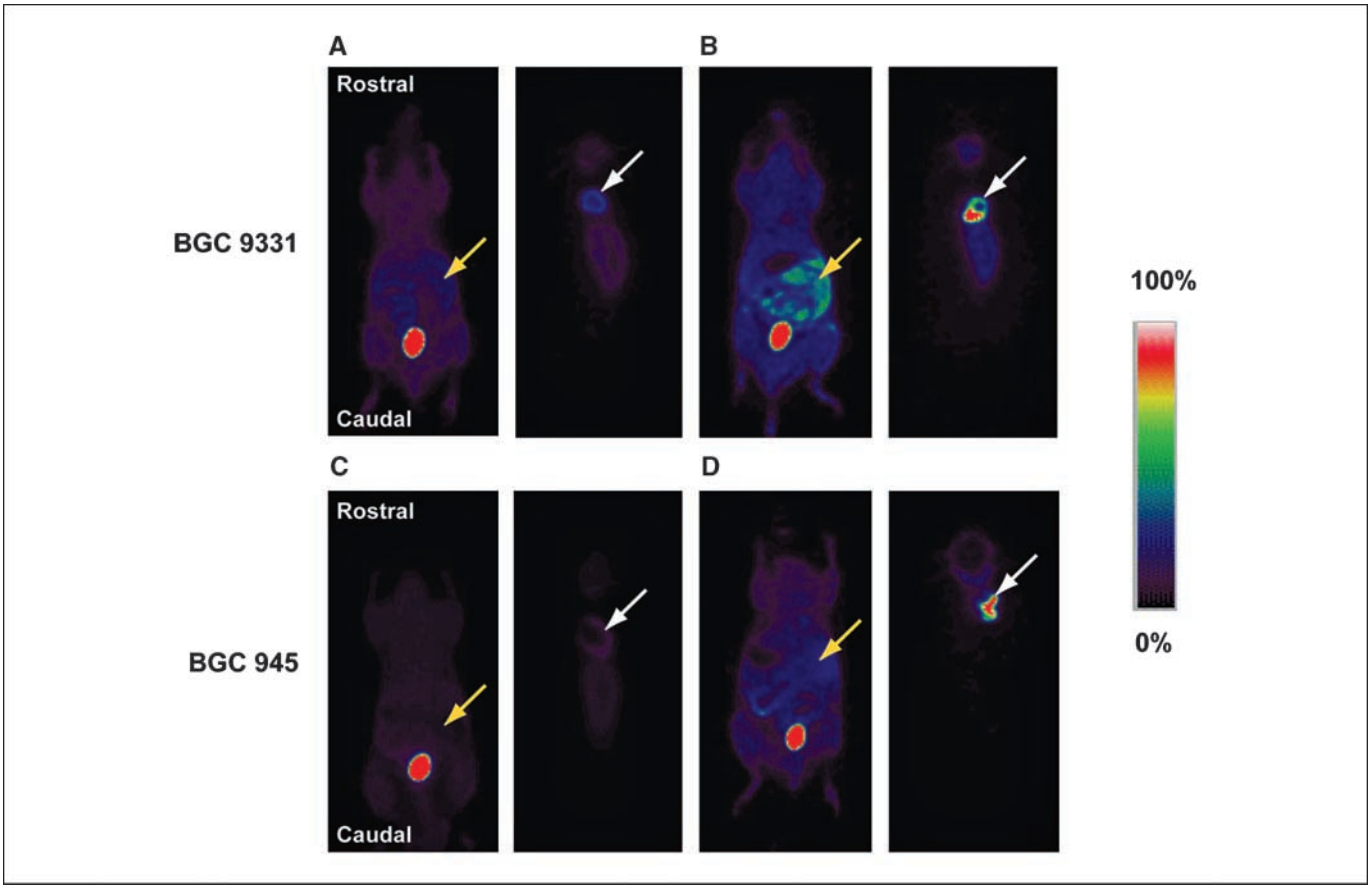

Figure 1. Typical 0.5-mm coronal [^{18}F]FLT-PET slices through the ventral (showing intestine and bladder) and dorsal regions (showing KB tumor) of control (*A* and *C*), 100 mg/kg BGC 9331–treated (*B*), and 100 mg/kg BGC 945–treated mice (*D*) imaged at 4 h posttreatment. The white and yellow arrowheads point to tumor and intestine, respectively, and bladder is seen as a high-intensity body in the caudal region of the mice. All images shown here were obtained from mice fed chow unsupplemented with folic acid. Note color bar.

Table 2. Time course and dose-response studies with BGC 9331

A. Time course

Tissue		Control	1 h	4 h	24 h	48 h
		$n = 4$	$n = 3$	$n = 5$	$n = 3$	$n = 3$
Tumor	AUC*	55 ± 9.2	109 ± 11 †	119 ± 2.8 †	42 ± 5.4	60 ± 7.9
	NUV60*	1.2 ± 0.22	3.0 ± 0.36 †	3.4 ± 0.12 †	1.0 ± 0.17	1.5 ± 0.13
	FRT60/2.5*	3.3 ± 0.18	7.7 ± 0.60 †	8.2 ± 1.1 †	4.3 ± 0.86	6.6 ± 2.8 ‡
Small intestine	AUC*	60 ± 10	102 ± 5.2 †	101 ± 17 †	67 ± 6.1	66 ± 4.2
	NUV60*	1.2 ± 0.18	2.6 ± 0.16 †	2.5 ± 0.52 †	1.3 ± 0.15	1.2 ± 0.11
	FRT60/2.5 †	1.8 ± 0.30	4.4 ± 2.3 †	3.5 ± 0.54 ‡	1.5 ± 0.22	1.4 ± 0.23
Brain	AUC	13 ± 0.61	16 ± 0.90	15 ± 2.4	13 ± 2.6	13 ± 1.6
	NUV60	0.25 ± 0.027	0.32 ± 0.028	0.30 ± 0.064	0.28 ± 0.041	0.26 ± 0.017
	FRT60/2.5 ‡	1.7 ± 0.29	2.4 ± 0.46 ‡	2.1 ± 0.16	2.0 ± 0.26	2.2 ± 0.17

B. Dose-response

Tissue		Control	50 mg/kg	100 mg/kg	150 mg/kg	200 mg/kg
		$n = 4$	$n = 6$	$n = 6$	$n = 3$	$n = 3$
Tumor	AUC*	55 ± 9.2	91 ± 9.6 †	119 ± 2.8 †	120 ± 33 †	146 ± 8.8 †
	NUV60*	1.2 ± 0.22	2.4 ± 0.41 †	3.4 ± 0.12 †	3.6 ± 0.95 †	4.4 ± 0.32 †
	FRT60/2.5*	3.3 ± 0.18	6.9 ± 2.6 ‡	8.2 ± 1.1 †	9.2 ± 1.1 †	8.9 ± 0.65 †
Small intestine	AUC †	60 ± 10	84 ± 20	101 ± 17 †	100 ± 1.9 ‡	101 ± 6.6 †
	NUV60 †	1.2 ± 0.18	1.8 ± 0.76	2.5 ± 0.52 †	2.4 ± 0.10 ‡	2.0 ± 0.48
	FRT60/2.5 †	1.8 ± 0.30	2.1 ± 1.1	3.5 ± 0.54 †	3.2 ± 0.25	2.5 ± 0.59
Brain	AUC ‡	13 ± 0.61	14 ± 1.5	15 ± 2.4	15 ± 0.45	18 ± 1.6 †
	NUV60	0.25 ± 0.027	0.33 ± 0.084	0.30 ± 0.064	0.32 ± 0.029	0.38 ± 0.0092
	FRT60/2.5	1.7 ± 0.29	2.6 ± 0.72	2.1 ± 0.16	2.5 ± 0.30	2.0 ± 0.43

NOTE: A summary of [^{18}F]FLT-PET pharmacokinetic variables in control and BGC 9331–treated KB tumor-bearing mice. Imaging studies were performed at different time points after mice (on standard diet) were treated with a single (100 mg/kg) dose of the drug (time course studies) or at 4 h after mice were injected with different doses of the drug (dose-response studies).

Data are mean ± SD.

One-way ANOVA (all groups; as superscript on variables) and multiple-comparison test against control values (Dunnett; as superscript on individual values).

*$P \leq 0.001$.

† $P \leq 0.01$.

‡ $P \leq 0.05$.

cell uptake of [^{3}H]Thd into KB cells, as well as its incorporation into the DNA in a concentration-dependent manner (Supplementary Fig. S1*A–D*). The effect was highest at 250 to 500 μg/mL (2-fold to 3-fold increase) in both whole cells and DNA (Supplementary Fig. S1*A-D*). Under the low folate culture conditions used, both BGC 9331 and BGC 945 had similar potencies for inducing [^{3}H]Thd uptake.

BGC 9331 and BGC 945 induce redistribution of ENT1 to plasma membrane. Because of a 1:1 stoichiometry between NBMPR and membrane ENT1 levels, the [^{3}H]NBMPR assay permits the number and affinity of membrane-associated ENT1 to be measured (18–20). With respect to the kinetics of [^{3}H]NBMPR uptake in KB cells, a drug concentration–dependent increase in the specific uptake of [^{3}H]NBMPR, i.e., the difference between the uptake of [^{3}H]NBMPR in the presence and absence of NBTG was seen (Supplementary Fig. S2*A* and *B*). A summary of the number of membrane ENT1 (B_{max}) and transporter affinity (K_D) are shown in Table 1. Both drug concentrations of BGC 9331 and BGC 945 significantly increased ENT1 B_{max} on KB cells; treatment of cells with 100 μg/mL of BGC 9331 or BGC 945 led to a 2-fold increase in ENT1 B_{max}. Under the conditions used, both BGC 9331 and BGC 945 had similar potencies for increasing B_{max}. In contrast, no relevant changes in transporter affinity were observed; the single unit change in K_D with BGC 9331 at the higher drug concentration is unlikely to be biologically significant. B_{max} and K_D were unchanged after pretreatment of cells with cyclohexamide, indicating that the effect was independent of intracellular protein synthesis.

BGC 945 selectively increases tumor but not intestine [^{18}F]FLT uptake *in vivo*. We used the Thd analogue [^{18}F]FLT and PET to determine the *in vivo* activity of the two TS inhibitors. In keeping with the *in vitro* findings above, both BGC 9331 and BGC 945 (100 mg/kg body weight, i.p.) induced an increase in [^{18}F]FLT-derived radioactivity in KB xenografts compared with tumors in vehicle-treated mice (Fig. 1*A–D*). Of interest to its

selectivity for FR, BGC 945 did not induce an observable change in intestinal radiotracer uptake, whereas BGC 9331 induced radiotracer uptake in this TS responsive normal tissue at 1 and 4 hours (Fig. 1*A–D*).

Summary radiotracer pharmacokinetic variables derived from quantitative analysis of BGC 9331–induced (100 mg/kg) time-dependent increases in tissue radioactivity are presented in Table 2A (see time versus radioactivity curves in Supplementary Fig. S3*A–C*). Under the conditions of this study, BGC 9331 increased tumor AUC, NUV_{60}, and FRT within 1 hour of drug injection. AUC, NUV_{60}, and FRT peaked at 1 to 4 hours, returning to baseline levels at 24 and 48 hours after drug treatment (Table 2A); comparative data obtained in small cohorts of mice fed chow unsupplemented with folic acid showed longer duration of action (≥24 hours) under these lower folate conditions (data not shown). With BGC 9331, the radiotracer uptake in intestine mirrored that of tumor (Table 2). Overall brain tissue had much lower radiotracer uptake, and no relevant changes in radiotracer accumulation were seen. Table 2B shows that the increase in AUC, NUV_{60}, and FRT was dose-related in tumor at the 4 hours time point; the effect was detectable at the first drug dose of 50 mg/kg reaching maximal levels at higher drug concentrations. The time course of radiotracer uptake into tumor as measured by [^{18}F]FLT-PET was slower after BGC 945 than with BGC 9331, peaking at 4 to 24 hours and returning toward baseline at 48 hours (Table 3A). In contrast to the radiotracer kinetics observed in tumor, there were no changes in AUC, NUV_{60}, or FRT in intestine after treatment with 100 mg/kg BGC 945 demonstrating selectivity for tumor; the change in brain radioactivity at 24 hours is unlikely to be biologically significant. The changes in AUC, NUV_{60}, and FRT induced by BGC 945 were detectable at a low dose of 25 mg/kg and showed a dose-related increase at 100 mg/kg (Table 3B). Unexpectedly, there was a reduction in the AUC and NUV_{60} variables at 200 mg/kg compared with that at 100 mg/kg. FRT remained high at this dose. Also of interest, at the dose of

Table 3. Time course and dynamic range studies with BGC 945

A. Time course

Organ		Control	1 h	4 h	24 h	48 h
		n = 8	*n* = 3	*n* = 3	*n* = 4	*n* = 4
Tumor	AUC*	57 ± 7.7	101 ± 21 †	116 ± 22 †	124 ± 26 †	65 ± 18
	NUV60*	1.3 ± 0.23	2.8 ± 0.73 ‡	3.2 ± 0.77 †	3.5 ± 0.90 †	1.6 ± 0.74
	FRT60/2.5	4.4 ± 2.0	7.5 ± 1.8	6.7 ± 0.52	8.4 ± 4.0	6.6 ± 4.1
Small intestine	AUC	66 ± 6.4	62 ± 6.8	69 ± 19	74 ± 12	58 ± 9.8
	NUV60	1.2 ± 0.14	1.1 ± 0.17	1.3 ± 0.51	1.3 ± 0.21	1.0 ± 0.20
	FRT60/2.5	1.2 ± 0.30	1.2 ± 0.22	1.4 ± 0.40	1.2 ± 0.37	1.3 ± 0.22
Brain	AUC ‡	15 ± 1.9	15 ± 2.1	16 ± 1.2	19 ± 2.0 ‡	15 ± 2.7
	NUV60	0.29 ± 0.046	0.28 ± 0.046	0.30 ± 0.041	0.37 ± 0.055	0.27 ± 0.048
	FRT60/2.5	1.9 ± 0.41	1.9 ± 0.21	1.8 ± 0.30	1.9 ± 0.36	1.8 ± 0.30

B. Dynamic range

Tissue		Control	25 mg/kg	100 mg/kg	200 mg/kg
		n = 8	*n* = 3	*n* = 3	*n* = 3
Tumor	AUC †	57 ± 7.7	67 ± 26	116 ± 22 †	62 ± 24
	NUV60 †	1.3 ± 0.23	1.8 ± 0.75	3.2 ± 0.77 †	1.8 ± 0.86
	FRT60/2.5	4.4 ± 2.0	5.3 ± 2.4	6.7 ± 0.52	8.3 ± 5.8
Small intestine	AUC	66 ± 6.4	67 ± 11	69 ± 19	83 ± 15
	NUV60	1.2 ± 0.14	1.1 ± 0.088	1.3 ± 0.51	1.7 ± 0.47
	FRT60/2.5	1.2 ± 0.30	1.0 ± 0.17	1.4 ± 0.40	2.4 ± 1.4
Brain	AUC	15 ± 1.9	16 ± 2.6	16 ± 1.2	15 ± 1.7
	NUV60	0.29 ± 0.046	0.33 ± 0.045	0.30 ± 0.041	0.31 ± 0.024
	FRT60/2.5	1.9 ± 0.41	2.3 ± 0.16	1.8 ± 0.30	2.3 ± 0.41

NOTE: A summary of [^{18}F]FLT-PET pharmacokinetic variables in control and BGC 945–treated KB tumor-bearing mice. Imaging studies were performed at different time points after mice (on folate-deficient diet) were treated with a single (100 mg/kg) dose of the drug (time course studies) or at 4 h after mice were injected with different doses of the drug (dynamic range studies).
Data are mean ± SD.
One-way ANOVA (all groups; as superscript on variables) and multiple comparison test against control values (Dunnett; as superscript on individual values).
*$P \leq 0.001$.
†$P \leq 0.01$.
‡$P \leq 0.05$.

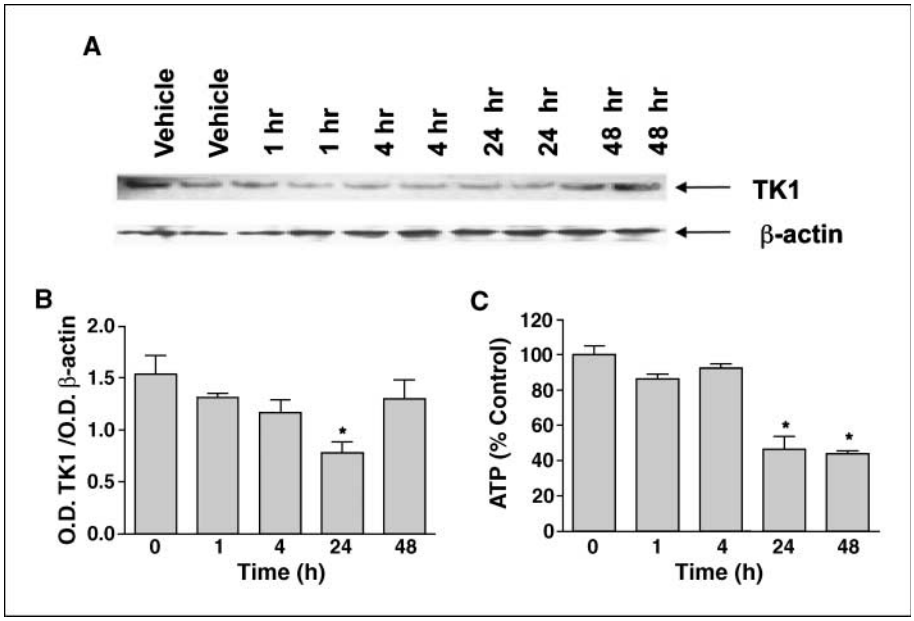

Figure 2. *A,* typical example of TK1 and β-actin (loading control) protein levels determined by Western blot at various time points after vehicle or 100 mg/kg BGC 945 treatment as described in Materials and Methods. *B,* summary data for TK1, which were expressed as ratios of the absorbance of TK1 to β-actin bands. *C,* summary data for ATP, determined with an *in vitro* bioluminescence kit as described in Materials and Methods and expressed as a percentage of vehicle control. *Points,* mean; *bars,* SD (n = 4 repeats). *, $P \leq 0.05$.

200 mg/kg, a detectable increase in intestinal radiotracer uptake was observed, although this did not reach statistical significance (P = 0.06 for all imaging variables; Table 3B).

TS-induced increase in [^{18}F]FLT uptake is not due to an increase in TK1 protein. To rule out increases in TK1/ATP being a contributing mechanism to the increase in [^{18}F]FLT uptake after TS inhibition and provide a clearer understanding of the time-dependent profile of antifolate drug effect, we assessed TK1 enzyme and ATP levels after BGC 9331 treatment in a cohort of mice (Fig. 2*A–C*). Rather than an increase, TK1 enzyme levels were unchanged within 4 hours of drug treatment and decreased significantly at 24 hours (P = 0.035) returning to baseline levels at 48 hours (Fig. 2*B*). ATP levels were also maintained for 4 hours but significantly decreased at 24 and 48 hours (Fig. 2*C*; P = 0.03).

Increases in [^{18}F]FLT uptake are associated with increases in tumor dUrd levels. The drug-induced increase in [^{18}F]FLT accumulation reported above were associated with increases in tumor dUrd levels (Fig. 3*A–C*). Tumor dUrd levels increased by 10-fold to 13-fold at the peak time of 1 to 4 hours after a 100 mg/kg BGC 9331 injection, returning to approximately control levels at 24 and 48 hours (Fig. 3*A*). The increase in dUrd levels after BGC 9331 was not clearly dose related (Fig. 3*B*). In keeping with the PET imaging studies, a small cohort of BGC 9331–treated mice fed chow unsupplemented with folic acid showed similar high-tumor dUrd levels at 4 and 24 hours (data not shown). A >10-fold increase in tumor dUrd was also seen after 100 mg/kg BGC 945, and this increase persisted for at least 24 hours (Fig. 3*C*).

Discussions

We have shown by [^{18}F]FLT-PET imaging that BGC 945 selectively inhibits TS in the α-FR–positive KB tumor but not in normal proliferating tissues at doses up to 200 mg/kg. Because TS, RFC, and other relevant targets of antifolate pharmacology are ubiquitously expressed in both tumor and normal proliferating tissues, antifolates rarely display high selectivity for tumors over normal tissues. The antifolate BGC 945, however, was designed to be transported into cells by the FR (11), which unlike the RFC, is highly expressed on a number of tumors coupled with a restricted functional expression on the apical surfaces of some normal tissues (3, 4). This implies that unlike classic antifolates (such as BGC 9331) that can be used to treat several tumor types, the utility of BGC 945 will be restricted to tumors expressing the FR. On the other hand, we will expect the therapeutic index with BGC 945 to be high as BGC 945 potently inhibits the growth of FR expressing cells under physiologic folate conditions (11). Antifolates like BGC 9331 also show high TS and growth inhibitory potencies in both FR and non-FR expressing cells. In this study, we sought to show relative selectivity of TS inhibition by BGC 945 in tumors over normal tissues using a clinically translatable imaging method.

We previously showed that TS inhibition is amenable to noninvasive imaging (8, 21). In the present report, we initially showed that both the relatively nonselective (BGC 9331) and the α-FR–selective (BGC 945) TS inhibitors possessed approximately equivalent intrinsic cellular potencies to increase nucleoside transport in the α-FR expressing human epidermoid KB tumor cells cultured under approximately physiologic folate conditions in a dose-dependent manner. We showed that [^{3}H]Thd uptake into whole cell and incorporation into DNA were enhanced by antifolate treatment. As with our previous studies with 5-fluorouracil (8), we confirmed that for both drugs the mechanism for enhanced nucleoside uptake could be explained at least in part by ~2-fold induction of ENT1 redistribution to the cell membrane. The process was not inhibited by cycloheximide and hence could not be attributed to increased ENT1 protein synthesis nor could it be attributed to increased expression of TK1 protein and ATP, as levels of these did not increase *in vivo*. The data could be further supported in the future by directly measuring TK1 enzyme activity levels.

As a prelude to clinical studies, we wanted to know if [^{18}F]FLT uptake increased with BGC 945 treatment and to determine an optimal imaging time for early clinical trials of the drug. With regard to developing appropriate/predictive tumor models, there are several challenges in the preclinical development of targeted antifolates like BGC 945. The first challenge is related to the

~5-fold higher plasma folate concentration in mice compared with humans (11, 12). To avoid competitive inhibition of BGC 945 binding to FR on KB tumors by folate, the mice were fed a diet unsupplemented with folic acid so as to achieve folate levels approximately that found in humans. Mice also have ~100-fold higher Thd levels than humans (6). The high Thd on one hand can reduce the overall uptake of the radiotracer, [^{18}F]FLT, in this species (22). We have, however, been able to show utility of the radiotracer for monitoring TS inhibition in mice despite the systematic reduction in absolute radiotracer uptake (8); this works in favor of humans because of their lower Thd levels (6, 23). Of relevance to the efficacy of TS inhibitors, the high Thd levels can bypass the effects of TS inhibition through the activity of TK1, making these models less predictive of human efficacy (12). The use of a TK-deficient tumor model can overcome this limitation. For example, treatment with BGC 9331 has been shown to be exquisitely efficacious in the TK-deficient mouse lymphoma tumor model, L5178Y TK$^{-/-}$ at doses of 10 mg/kg due to the inability of this tumor to salvage Thd (14). The same model cannot be used to study efficacy of BGC 945, however, due to its lack of FR expression. Furthermore, even with the L5178Y TK$^{-/-}$ model, therapeutic index cannot be easily assessed as dThd salvage is still in operation in normal tissues. Because of these challenges in transferring knowledge of preclinical efficacy of antifolates into clinical development, we decided to compare our imaging readout to another biomarker of TS inhibitory activity, dUrd.

Inhibition of TS leads to an increase in dUMP and dUrd in proliferating cells (24), and an increase in dUrd can be detected in mice and in humans after administration of TS inhibitors (4, 5). Plasma dUrd is therefore a useful PD marker of TS inhibition in proliferating tissue, such as gut, bone marrow, and tumor. We have adapted the assay to specifically measure tumor dUrd to assess localized TS inhibition. For both BGC 9331 and BGC 945, tumor dUrd increased ~10-fold in a time-dependent fashion. This effect was not dose-related at 4 hours after BGC 9331 injection, consistent with our previous experience.[4] This may be due to the dynamics of dUrd in tissues and plasma—efflux mechanisms, feedback loops, and systemic elimination. Because we did not directly measure TS inhibition but rather changes in dUrd levels as a surrogate for TS inhibition, the lowest level of TS inhibition that shows an increase in FLT uptake is unknown. Dose dependence changes of dUrd after BGC 945 was not assessed in this present study. BGC 9331 at 100 mg/kg induced an increased radiotracer accumulation in both tumors and small intestines as shown by [^{18}F]FLT-PET, and this effect was dose related. NUV_{60}, AUC, and FRT all peaked at 1 to 4 hours and returned toward baseline at 24 hours demonstrating rapid onset and relatively short duration of action. This short duration of action was expected, as BGC 9331 does not undergo polyglutamation and therefore has rapid elimination in mice. In contrast, at an equivalent dose of 100 mg/kg, BGC 945 induced increased radiotracer accumulation in tumor but not intestine demonstrating tissue specificity. This tissue specificity was not due to the different dietary conditions used, because mice on chow unsupplemented with folic acid treated with BGC 9331 showed similar increased radiotracer uptake in intestine (data not shown). For BGC 945, NUV_{60}, AUC, and FRT peaked at 4 to 24 hours and returned toward baseline at 48 hours. Gibbs et al. have reported that BGC 945 is rapidly cleared from mouse plasma but retained in KB tumors with a terminal half life of 28 hours (11). Provided that the pharmacokinetics of BGC 945 in humans is such as that to permit sufficient drug accumulation in tumors, ~24 hours will be the ideal time for imaging FR-mediated TS inhibition in humans with the PET technology.

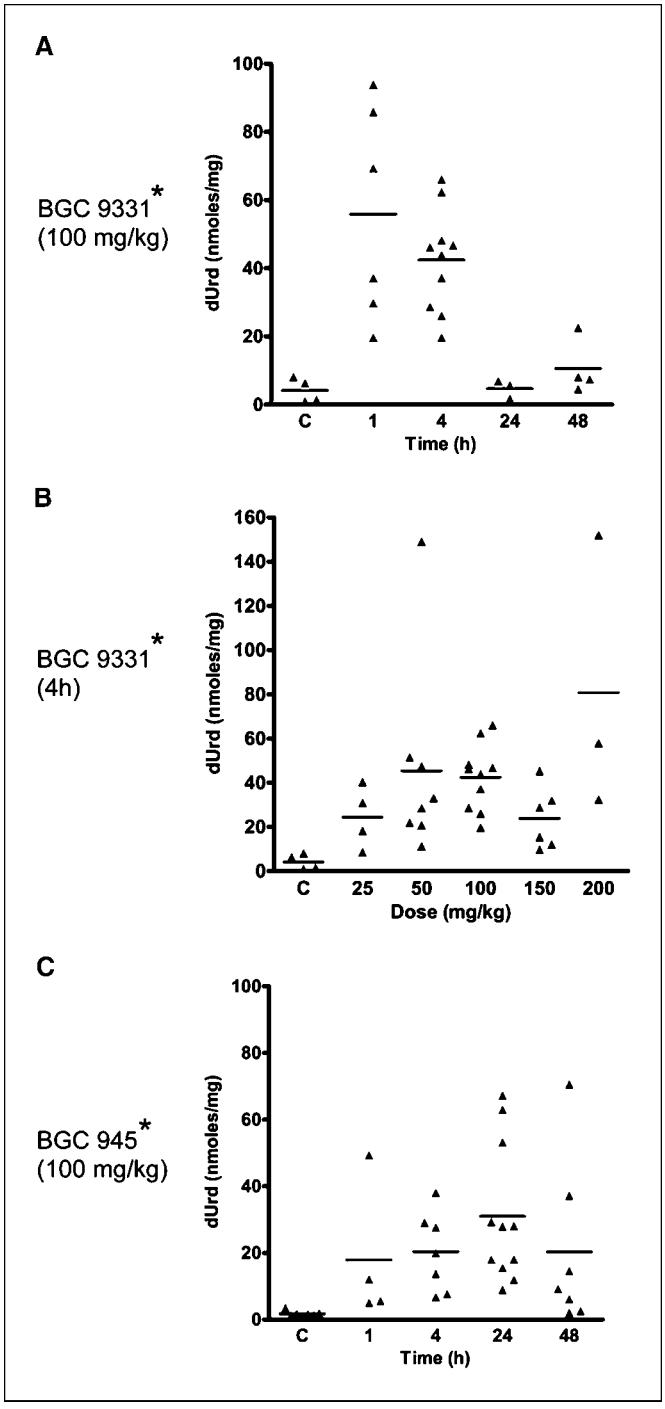

Figure 3. dUrd levels in mouse KB tumors after treatment with BGC 9331 or BGC 945. *A,* BGC 9331 time dependence (standard chow). *B,* BGC 9331 dose-dependence (standard chow). *C,* BGC 945 time-dependence (chow unsupplemented with folic acid). The levels of dUrd were measured by HPLC as described in Materials and Methods. Data are individual mouse tumor dUrd levels and mean (*solid line*). *, $P \leq 0.05$.

[4] Unpublished data.

Given that toxicities from antifolates (25), including myelosuppression and diarrhea, are related to their effects on normal proliferating tissue, our PET findings for BGC 945–treated mice are strongly indicative of a high (biomarker-based) therapeutic index in subjects with FR-positive tumors. [^{18}F]FLT-PET may have utility for predicting activity in tumors or subclinical normal tissue toxicity. Drug doses that induce measurable [^{18}F]FLT uptake may be used define the biologically effective dose. On the other hand, a detectable, but nonsignificant, increase in intestinal [^{18}F]FLT accumulation was observed with BGC 945 at 200 mg/kg that may be attributed to transient TS inhibition in normal proliferating tissue induced by non-FR uptake when drug levels are high; this can be used as a basis to define subclinical toxicity (although the exact relationship between the extent of TS inhibition in normal tissues and gastrointestinal toxicity is unknown and will need to be assessed clinically). With respect to imaging variables, we found that NUV_{60}, AUC, and FRT were useful variables for assessing TS inhibition at and below 100 mg/kg of BGC 945. The reduction in tumor NUV_{60} and AUC at 200 mg/kg was unexpected and inconsistent with the *in vitro* cell culture [^{3}H]Thd studies, where high doses led to a plateau in radiotracer uptake. We speculate that the reduction in NUV_{60} and AUC at this very high dose is due to nonspecific effect of the drug on radiotracer delivery. This assertion is supported by the absence of a reduction in the FRT variable. FRT, a variable that describes the fraction of radiotracer reaching a tissue that is retained, was still high at 200 mg/kg dose, indicating utility of this variable at such high doses. Of note, only single-dose pharmacodynamic changes were assessed in this report. The technology may have limitations when used after repeat dosing with antifolate TS inhibitors as decreases in [^{18}F]FLT accumulation reflecting a reduction in proliferation, and hence, TK1 enzyme activity can occur under such conditions (16, 17, 21).

In summary, we have used [^{18}F]FLT-PET imaging to show tumor-specific TS inhibition by BGC 945 and shown that a likely mechanism by which [^{18}F]FLT-PET measures TS inhibition involves redistribution of nucleoside transporters to the cell membrane. Depending on the pharmacokinetics of BGC 945 in humans, clinical studies should consider a protocol involving a baseline [^{18}F]FLT-PET scan followed by another [^{18}F]FLT-PET scan in the same patient at ~24 hours after drug treatment when peak effects are seen.

Disclosure of Potential Conflicts of Interest

A.L. Jackman: Consultant, BTG International. The other authors disclosed no potential conflicts of interest.

Acknowledgments

Received 1/11/2008; revised 2/21/2008; accepted 3/11/2008.

Grant support: Research United Kingdom grants CA2536/A4892, CA2536/A5708, and C1323/A7691, and UK Medical Research Council core grant.

The costs of publication of this article were defrayed in part by the payment of page charges. This article must therefore be hereby marked *advertisement* in accordance with 18 U.S.C. Section 1734 solely to indicate this fact.

We thank BTG International Ltd. for kindly providing BGC 9331 and BGC 945.

References

1. Gibbs JB. Anticancer drug targets: growth factors and growth factor signalling. J Clin Invest 2000;2000:9–13.
2. Henderson EA, Bavetsias V, Theti DS, Wilson SC, Clauss R, Jackman A. Targeting the α-folate receptor with cyclopenta[g]quinazoline-based inhibitors of thymidylate synthase. Bioorg Med Chem 2006;14:5020–42.
3. Kelemen LE. The role of folate receptor a in cancer development, progression and treatment: cause, consequence or innocent bystander? Int J Cancer 2006;119:243–50.
4. Parker N, Turk MJ, Westrick E, Lewis JD, Low PS, Leamon CP. Folate receptor expression in carcinomas and normal tissues determined by a quantitative radioligand binding assay. Anal Biochem 2005;338:284–93.
5. Jackman AL, Theti DS, Gibbs DD. Antifolates targeted specifically to the folate receptor. Adv Drug Deliv Rev 2004;56:1111–25.
6. Li KM, Rivory LP, Hoskins J, Sharma R, Clarke SJ. Altered deoxyuridine and thymidine in plasma following capecitabine treatment in colorectal cancer patients. Br J Clin Pharmacol 2007;63:67–74.
7. Mitchell F, Lynn S, Jackman AL. Modified high-performance liquid chromatography assay for the measurement of 2′-deoxyuridine in human plasma and its application to pharmacodynamic studies of antimetabolite drugs. J Chromatogr B 2000;744:351–8.
8. Perumal M, Pillai RG, Barthel H, et al. Redistribution of nucleoside transporters to the cell membrane provides a novel approach for imaging thymidylate synthase inhibition by positron emission tomography. Cancer Res 2006;66:8558–64.
9. Oh SJ, Mosdzianowski C, Chi DY, et al. Fully automated synthesis system of 3′deoxy-3′[^{18}F]fluorothymidine. Nucl Med Biol 2004;31:803–9.
10. Theti DS, Bavetsias V, Skelton LA, et al. Selective delivery of CB300638, a cyclopenta[g]quinazoline-based thymidylate synthase inhibitor into human tumor cell lines overexpressing the a-isoform of the folate receptor. Cancer Res 2003;63:3612–8.
11. Gibbs DD, Theti DS, Wood N, et al. BGC 945, a novel tumor-selective thymidylate synthase inhibitor targeted to α-folate receptor-overexpressing tumors. Cancer Res 2005;65:11721–8.
12. van der Wilt CL, Backus HH, Smid K, et al. Modulation of both endogenous folates and thymidine enhance the therapeutic efficacy of thymidylate synthase inhibitors. Cancer Res 2001;61:3675–81.
13. Ford HER, Mitchell F, Cunningham D, et al. Patterns of elevation of plasma 2′-deoxyuridine, a surrogate marker of thymidylate synthase (TS) inhibition, after administration of two different schedules of 5-fluorouracil and the specific TS inhibitors raltitrexed (Tomudex) and ZD9331. Clin Cancer Res 2002;8:103–9.
14. Jackman AL, Kimbell R, Aherne GW, Brunton L, Jansen G, Stephens TC. Cellular pharmacology and *in vivo* activity of a new anticancer agent, ZD9331: a water-soluble, nonpolyglutamatable, quinazoline-based inhibitor of thymidylate synthase. Clin Cancer Res 1997;3:911–21.
15. Workman P, Twentyman P, Balkwill F, et al. United Kingdom coordinating committee on cancer research (UKCCCR) guidelines for the welfare of animals in experimental neoplasia (second edition). Br J Cancer 1998;77:1–10.
16. Barthel H, Cleij MC, Collingridge DR, et al. 3′-Deoxy-3′-[^{18}F]fluorothymidine as a new marker for monitoring tumor response to anti-proliferative therapy *in vivo* with positron emission tomography. Cancer Res 2003;3:3791–8.
17. Leyton J, Latigo JR, Perumal M, et al. Early detection of tumor response to chemotherapy by 3′deoxy-3′-[^{18}F]fluorothymidine positron emission tomography: the effect of cisplatin on a fibrosarcoma tumor model *in vivo*. Cancer Res 2005;65:4202–10.
18. Lay-Beng GOH, Chee-Wee L. Reduction of equilibrative nitrobenzylthioinosine-sensitive nucleoside transporter in tamoxifen-treated MCF-7 cells: an oestrogen-reversible phenomenon. Biochem J 1997;327:31–6.
19. Boleti H, Coe IR, Baldwin SA, Young JD, Cass CE. Molecular identification of the equilibrative NBMPR-sensitive (es) Nucleoside transporter and demonstration of an equilibrative NBMPR-insensitive (ei) transport activity in human erythroleukemia (K562) cells. Neuropharmacology 1997;36:1167–79.
20. Hammond JR. Interaction of a series of draflazine analogues with equilibrative nucleoside transporters: species differences and transporter subtype selectivity. Arch Pharmacol 2000;361:373–82.
21. Yau K, Price P, Pillai RG, Aboagye EO. Elevation of radiolabelled thymidine uptake in RIF-1 fibrosarcoma and HT29 colon adenocarcinoma cells after treatment with thymidylate synthase inhibitors. Eur J Nucl Med Mol Imaging 2006;33:981–7.
22. van Waarde A, Cobben DC, Suurmeijer AJ, et al. Selectivity of ^{18}F-FLT and ^{18}F-FDG for differentiating tumor from inflammation in a rodent model. J Nucl Med 2004;45:695–700.
23. Nottebrock H, Then R. Thymidine concentrations in serum and urine in different animal species and man. Biochem Pharmacol 1977;26:2175–9.
24. Webley SD, Welsh SJ, Jackman AL, Aherne GW. The ability to accumulate deoxyuridine triphosphate and cellular response to thymidylate synthase (TS) inhibition. Br J Cancer 2001;85:446–52.
25. Plummer R, Rees C, Hughes A, et al. A Phase I trial of ZD9331, a water-soluble, nonpolyglutamatable thymidylate synthase inhibitor. Clin Cancer Res 2003;9:1313–22.